DNIPRO UNIVERSITY of TECHNOLOGY 1899

Mining of Mineral Deposits

Volume 15 (2021), Issue 3, 62-70

MMD JOURNAL / MINING.IN.UA

UDC 622.83

https://doi.org/10.33271/mining15.03.062

Early assessment of seismic hazard in terms of Voronezh massif-Moscow Depression contact

Igor Movchan[1*], Alexandra Yakovleva[1], Alexander Movchan[2], Zilya Shaygallyamova[1]

[1]*Saint Petersburg Mining University, Saint Petersburg, 199106, Russian Federation*
[2]*University of Liverpool, Liverpool, L69 3BX, United Kingdom*

**Corresponding author: e-mail Movchan_IB@pers.spmi.ru*

Abstract

Purpose is to develop a system approach for early assessment of areas being of high seismic hazard and characterizing by low stability of rock mass relative to external loads.

Methods. Well cores have been assessed down to 30 depth and seismic observations have been accumulated. Complexes of field geophysics methods have been applied for the research as well as remote sensing materials, digital model of surface relief, and techniques of qualitative and quantitative interpretation.

Findings. Seismic hazard map has been formed in terms of seismic intensification and ground displacement units. The abovementioned is quite reliable but a cost-based result involving early assessments of high seismic hazard areas to infill network of geophysical measurements in the neighbourhood of the areas for their further quantitative characterization. It has been identified that rare well network and definite geophysical lines, run under conditions of a complex terrain, cannot localize the areas of high seismic hazard to focus builders on the enforcement of certain components of the erected structures. It has been defined that end result of the prognostic developments takes a shape of mapping of local areas with the decreased stability of upper share of the geological section supported by further measurements by means of a common depth point method (CDP). Comparison of potential secondary earthquake sources with high permeability zones makes it possible to predict highly reliable areas of the increased seismic magnitude.

Originality. For the first time, interpretation techniques have been adapted to describe parametrically nonpotential geofields (i.e. optical density of remote basis; and relative elevation), accepted during the steps of potential field processing, with the use of wave analogies.

Practical implications. The methods have been developed helping optimize field geological and geophysical operations in terms of area and well number as well as measuring stakes under the conditions of the limited prior data amount.

Keywords: *jointing, seismic zoning, terrain, karst, digital model, interpretation*

1. Introduction

The investigated area is located on the joint of two Precambrian structures – the northern slope of Voronezh massif and the southern slope of Moscow Depression (Central Russian syneclise). In addition, it is mapped within the periphery of large circular geological structure being 250 km in diameter. The circular structure is observed within the territory of Tula and Oryol Regions (Tula dome and ring structure) coinciding with significant part of Central Russian Upland (Fig. 1a) [1]. Hypothetically, dome-shaped formations result from generation of hot spot or, in other words, the impact of endogenous plume. On the Earth's surface, similar vertical motion of plumes is often correlated with the elevations; along their periphery, they are limited by ring and concentric faults, including deep ones. The processes are complicated by the formation of set of different-order linear tectonic faults, which form, in particular, fairly branched network in Tula Region. A regional linear fracture with latitudinal direction, crossing through the entire Oka basin [2] and including Tula and Shchekino settlements, is the most famous of them (Fig. 1b). There are few kilometers from Shchekino to the area of the planned construction. Another northeast-directed regional fault is in the eastern part of Tula Region. Approximately, it is propagated along the line of Efremov, Uzlovaya, Novomoskovsk, and Venev Towns. Probably, the fault originates from the Mediterranean coast tracing in the Russian Federation territory north-easterly up to Yamal Peninsula.

Despite Tula Region location in the zone of low-intensity seismic responses and rather far from the epicenters of earthquakes, registered in Alpine belt, seismic activity cannot be negligible within the area.

Received: 1 April 2021. Accepted: 3 August 2021. Available online: 22 September 2021

Published by the Dnipro University of Technology on behalf of Mining of Mineral Deposits. ISSN 2415-3443 (Online) | ISSN 2415-3435 (Print)

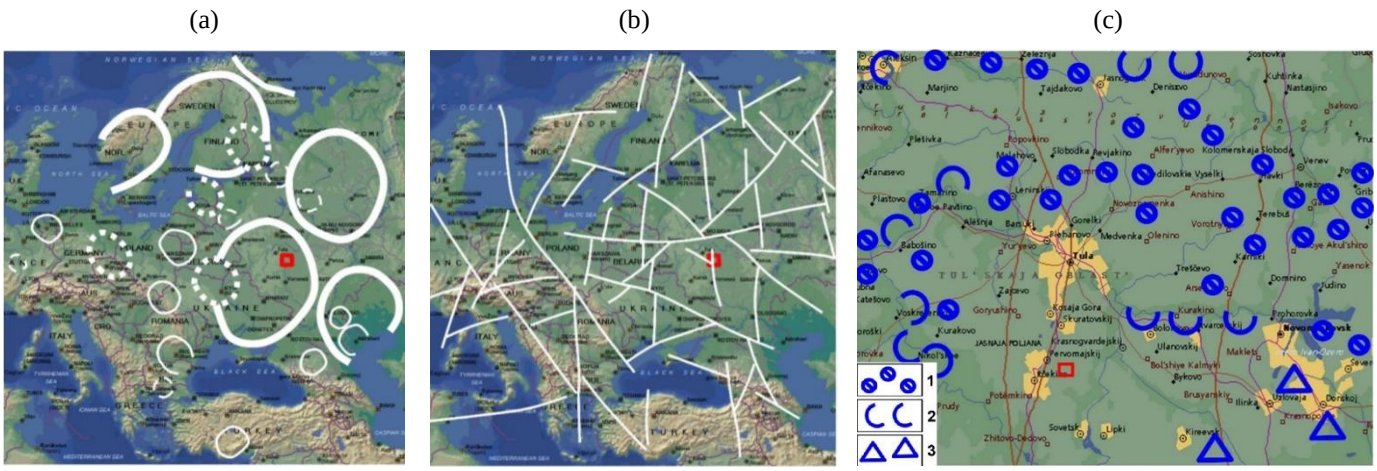

Figure 1. Geostructural position of the analyzed area (according to V.N. Brykhanov, V.A. Boosh and A.G.Chikishev): (a) schematic map of regional circular formations of 1st-4th orders within the contact of the East-European platform, West-European plate and Mediterranean belt; (b) schematic map of regional lineaments in the area of the contact. The approximate position of the analyzed territory is marked by red line; and (c) fragment of regional map of engineering and geological zoning of Tula Region and adjacent territories (according to Popov [3]); 1 – karst; 2 – landslide phenomena; 3 – areas of subsidence process development. The analyzed area is located slightly south of Tula where the processes of karst formation and vertical subsidence of upper part of geological cross-section are also observed

The idea is supported indirectly by morphology of general seismic zoning map (GSZ-2015-C: the shaking period is almost 5000 years with 1% probability of the calculated seismic intensity exceeding within 50 years) [4]-[6]. Though in the vicinity of the analyzed object the map is of monotonic and low-intensity structure, there is the gradient zone from 5 to 6-7 scores of Richter scale at the distance of about 130-140 km. Seeing the strike of anomalous seismic zones in sublatitudinal or in northeastern directions, one can suppose their genetic relationship with regional disjunctive faults mentioned above.

Vertical cross-section of the region [7] is characterized by monoclinal bedding of SCC with nonconformity at the junction of Vendian, Archean-Proterozoic formationsб and Devonian deposits. In the relief of the stratified rock massif contacts, the synform and Vendian layer thinning in the vicinity of investigated area can be observed. The feature of geological structure is supposed to be the marker of deep regional faults crossing directly the territory and being inherited by structural anomalies. Moving up through the cross-section, thick Devonian deposits as well as Carboniferous formations can be noted, including widespread limestone, caused karst formation and, as a result, vertical subsidence risk during interaction of near-surface SCC with elements of fracture tectonics.

Karst phenomena observed north and south of Tula City [8]-[11] are mainly caused by interaction between groundwater and Mississippian limestone as well as Devonian gypsum (Fig. 1c). Karst in Upper Devonian gypsum is especially intensive. In the context of the analyzed region, the karst is observed in various forms: as sinkholes; hollows; gullies; karst lakes; disappearing rivers; coastal depressions; karst depressions; niches; and underground voids. The intensity of karst development is assessed by the area of its manifestation and specific volume of the mapped karst cavities. This intensity is higher in Tula Region compared to neighbouring territories owing to greater fragmentation and relatively high fracturing of carbonate strata. The dependence of karst formation both on dynamics of endogenous fracture tectonics and exogenous factors [12]-[14] bring about continuous dynamics of karst development and nonzero hazard of new vertical subsidence under the fast healing of karst formations implying the relevance of geodynamic evaluation of area [10], [15], [16]; it especially under conditions of extensive mine workings, which are observed within the investigated object. Previously, the authors have analyzed seismogenic hazard in the vicinity of geodynamically active geoblocks because of activation of fault tectonics under conditions of hydraulic fracturing [17] with application of non-potential geofields. The paper presents the extension of systematic approach to the analysis of these geofields within geodynamically stable Earth's crust.

2. Methods

The key element of database is remote sensing data combined with digital model of the Earth surface elevations (DME), including, in particular, aerophotos and satellite images of the terrain. They are defined as scaled-down model of terrain where geological and structural anomalies are encoded in combinations of landscape components; the combinations are encoded in the set of half-tone photo anomalies. Geological heterogeneities, which are not explicitly observed at the surface due to masking by soil and vegetation cover, intensifying both weathering processes and anthropogenic influences, are clearly manifested in remote sensing data. Physically, this is explained by evolutionary process of landscape formation within the considered territory where all landscape components depend functionally on geological heterogeneities. At the stage of expert decoding [18], the lineament field is reconstructed both with remote sensing data and DME for reliable verification of result. The lineament as linearized (straightened) landscape element is traced through heterogeneous forms of half-tone anomalies in remote sensing data and heterogeneous forms of relief to map the elements of fracture tectonics getting the latest activation [16], [19]. Expert decoding is based on visual estimations and manual, little-automated operations with one or the set of the most contrasting spectrum bands. In this context, the contrast is defined traditionally as the parameter:

$$K = \frac{(B_2 - B_1)}{B_2},\ 0 < K < 1, \qquad (1)$$

computed by the values of optical density field between pair of neighboring objects and averaged over the entire considered area.

Scalar fields of parameters, derived from the initial scalar field by means of application of differential operators and estimation of exponential parameters, are a hint in monitoring the results of expert decoding. The calculation of shadow forms of geofield surface $f(x, y)$, when this surface is illuminated by homocentric source [20], can be defined as the simplest transform of the kind. If β is an angle, formed by the incident ray and the horizon plane, then γ is an angle between the conditional direction to the north and the projection of incident ray onto the horizontal plane, counted clockwise as well as:

$$\varphi = \arctan\left(\left(\frac{\partial f}{\partial x}\right)^2 + \left(\frac{\partial f}{\partial y}\right)^2\right), \tag{2}$$

being the slope angle of virtual surface of geofield, and:

$$\phi = \left(\arctan\left(\frac{\partial f}{\partial y} - \frac{\partial f}{\partial x}\right)\right)^2, \tag{3}$$

being the angular sector of view, where:

$$\frac{\partial f}{\partial x} = \frac{(f_{31} + 2f_{32} + f_{33}) - (f_{11} + 2f_{12} + f_{13})}{8K_s}; \tag{4}$$

$$\frac{\partial f}{\partial y} = \frac{(f_{13} + 2f_{23} + f_{33}) - (f_{11} + 2f_{21} + f_{31})}{8K_s}, \tag{5}$$

$K_S = 9$ is the number of matrix elements composed by values of geofield in sliding window:

$$3\times3\begin{pmatrix} f_{11} & f_{12} & f_{13} \\ f_{21} & f_{22} & f_{23} \\ f_{31} & f_{32} & f_{33} \end{pmatrix}, \tag{6}$$

then the shadow forms of geofield surface are represented by the parameter:

$$S_R = 255\big(\cos(90-\alpha)\cdot\cos(\varphi) + \\ +\sin(90-\alpha)\cdot\sin(\varphi)\cdot\cos(\gamma-\phi)\big). \tag{7}$$

Contrasting of local half-tone structures is implemented by preliminary application of differential operators, for example, the Sobel operator [21], [22] used in the convolution mode in 3×3 window with the next transfer function:

$$\Omega_x\begin{pmatrix} -1 & -2 & -1 \\ 0 & 0 & 0 \\ 1 & 2 & 1 \end{pmatrix} \text{ and } \Omega_y\begin{pmatrix} -1 & 0 & 1 \\ -2 & 0 & 0 \\ -1 & 0 & 1 \end{pmatrix}, \tag{8}$$

The result of recalculation is assigned to the center of sliding window.

Left transfer function contrasts with the geostructural lines of sublatitudinal strike; and right transfer function underlines geostructures of submeridional strike (Fig. 2a, and 2b). Another example is borrowed from thermodynamics (Fig. 2c) and reflects the ratio of ordered components of geofield against disordered (chaotic) components in the structure of scalar field (Fig. 2c) [23], [24]:

$$H = -\sum_{i=1}^{n}\left(p_i \cdot \log_2 p_i\right), \tag{9}$$

where:

p_i – the probability of i^{th} state of a physical system (in practice, it is frequency of i^{th} state implementation described as the interval of field values between two adjacent isolines).

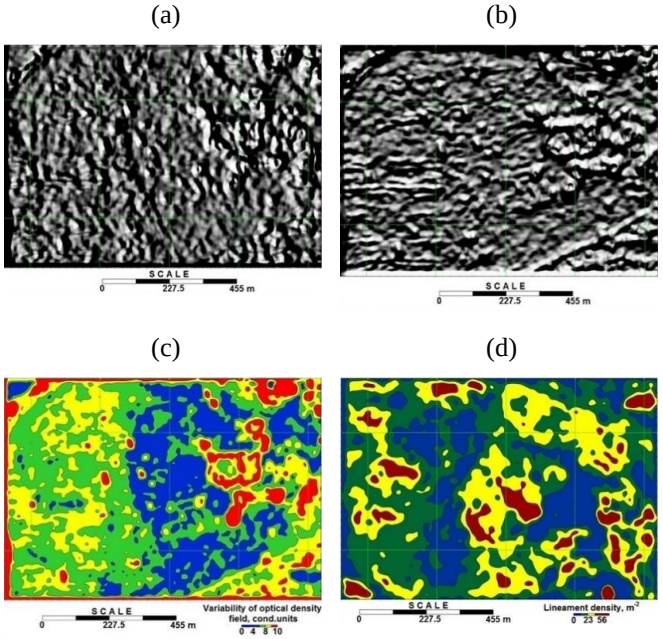

Figure 2. Recalculation example of remote sensing data and digital elevation model into a form demonstrating clearly both position and orientation of the linear (geodynamic) zones: (a) and (b) the result of applying differential operators to digital elevation model for contrasting the positions of geodynamic zones of different strike azimuths (northwest and northeast respectively); (c) characterization of disorder degree (entropy) of optical density field of the considered area; and (d) a field of lineaments density (fragmentation degree of an upper part of the cross-section) of the survey area (Shchekinsk District, Tula Region)

The key procedure in the applied system of transforms is developed in terms of the project in the automated lineament analysis accompanying and verifying expert lineament decoding. The algorithm includes searching for extremum points in the system of values of initial scalar field as well as in the system of values of the calculated field of horizontal gradient modulus. Following procedure is rotation of elementary lineaments around each of mentioned points based on standard rotation matrix and local spline interpolation. Final strike azimuth of particular lineament is selected by a minimum criterion of the dispersion functional. The result of such recalculation is represented by the set of coaxial structures derived by generalization procedure. The latter is represented, first of all, by a statistical sorting of one-oriented structures with elimination of quasiperiodic lineament nets. Three standard procedures form the presorting basis: determination of direction rose of isolines of scalar field based on the structure of autocorrelation function; estimation of variance of strike azimuths of local lineaments; and elimination of the set of elementary lineaments with the highest strike

azimuth variances. The second component of generalization procedure includes combining the tips of the nearest coaxial lineaments into macroscopic straightened structures (geostructural lines) with the subsequent smoothing of these structures. The algorithm also includes such logical procedures as elimination of "blind" intersection of lineament structures of different azimuths as well as the priority of extended linear elements in comparison with arch concentric elements. The generalization of results of lineament decoding in the form of map of lineament density distribution is important operation for final interpretation. Since the methodological foundations of seismic hazard maps are based on direct analogy between lineaments and fracture tectonics [3], [25], the increasing lineament density can be correctly interpreted as increasing fragmentation of upper part of cross-section. Numerically, the procedure is based on counting the number of tips of selected lineaments per unit area of integration interval (Fig. 2d).

Morphotectonic analysis is independent operation verifying the abovementioned morphostructural reconstructions and information about position of reduced stability areas in an upper part of the cross-section. At this point, the basic element includes the selection of geoblock boundaries, in which, firstly, the expert analysis of anomalies of spatial stationarity parameter (entropy parameter) and, secondly, the optimal separation of this signal into long-wave and short-wave components are applied. The expert analysis of the scalar entropy field is performed visually with involvement of contour lines and half-tone images of entropy anomalies. The principal elements of morphostructural zoning include the existence of isometric and/or elongated anomalies, fixation of their linear size, the dominant strike azimuth of axes of anomalies and\or local gradient zones, existence of zones of sharp space-related gradient, variation of general "image" of isolines, variation of space-related stationarity of signal, and existence of significant jog in the structure of individual isolines or set of isolines. Separation of signal into components is initially associated with a methodological element for identifying the base and erosion-active layers in the terrain structure. In the considered case, it is enough to select the threshold wavelength (space-related frequency) of the signal separating the spectrum of this signal into two areas with fundamentally different harmonics structures. The distribution of threshold wavelength along the coordinate axes can differ in remarkable anisotropy. This is marked by azimuthal variation of autocorrelation radius approximated by elliptical contour. As a consequence, the signal separation by wavelength is reduced to averaging in sliding elliptical window with semiaxes being equal to autocorrelation radius in two mutually orthogonal directions. Finally, the extended elements are traced in the structure of components with different wave lengths λ, correlated with a priori known manifestations of fracture tectonics, appeared at different depths.

The system of the abovementioned estimations is completed by deep geostructural reconstructions based on the analysis of landforms of the Earth's surface. Paper [17] considers physical foundations of the method and their correspondence to geological and engineering formulation of the problem. The main idea is to interpret availability of periodic and quasiperiodic components in the structure of spatial geological and geophysical signal by the standing wave shaping:

$$K(x) = A \cdot \cos(kx) \cdot \cos(\omega t - \phi), \quad (9)$$

in a spatial structure of nonequilibrium geological media [26], [27] The wave dynamics is caused by periodic transgressive and regressive processes; regular tectonic and magmatic activations, covering both the entire Earth's crust; and particular small vicinity of point within the considered geoblock. Since the geological environment is a spatially distributed system, the recorded vibrations of its individual elements can propagate in the volume of rock complexes forming the waves. In particular, within the layered rock massif they are recorded as an alternation of synforms and antiforms with definite step in the relief of interface between any pair of structural and constitutional complexes. In other words, the wave image to structure mining environment is extremely real approximation of phenomena associated with nonequilibrium distribution of heterogeneities.

Analytical continuation of potential and nonpotential geosignals into the area of geological or technogenic heterogeneities (the source of geofield anomalies) under such a model is equivalent to the transition to areas with increasing surface tension force leading to the suppression of short-wave and low-amplitude components. If the geofield is given by spatial distribution of absolute heights of the Earth's surface relief then under conditions of its noticeable differentiation and small anthropogenic change, individual elements of the geofield are hydrostatically (isostatically) compensated in the volume of geological environment. Consideration of the general arguments helps conclude that the process of hydrostatic compensation of positive and negative landforms is confirmed to the extent of geochronological scale when the rocks are characterized by elastoplastic dynamics being similar to the viscous fluid dynamics [28], [29]. As a result, according to the skin effect, the larger shape of the Earth's relief corresponds to the deeper hydrostatic compensation which conforms to the ideas abovementioned concerning the growth of surface tension forces as the function of depth.

3. Results of geostructural reconstructions

The standard method to process data of different scales, taking into account significant anthropogenic influences on the landscape and masking the terrain due to Quaternary structural and constitutional complex and vegetation cover was applied for the analysis. Smaller scale of remote sensing images corresponds to lower amplitude of anthropogenic impact on modern landscape as well as to more contrasting responses of fracture tectonics elements in the optical density field of remote sensing data and digital elevation model. Thus, satellite image of regional scale amounting to almost 1:200000 (Fig. 3a) reflects the elements of planetary fractures being masked directly at the surface and getting definite peculiarities. One can see three systems of regional geodynamic zones: sublatitudinal, submeridional, with northeastern strike. First, they are of quasiperiodic nature; second, each linear structure is of small curvature. The structure of northwestern strike azimuth with high contrast of manifestation on remote image has aperiodicity and significant curvature that define its confinedness to suture geoblock zone. As Figure 3c shows, the zone may reflect the response in modern landscape of the main fault which complicates southwestern flank of Pachelm Trough [30]. With regard to submeridional geodynamic zone, there is the effect of shear displacement of elements of geodynamic zone of northwestern strike within the analyzed area.

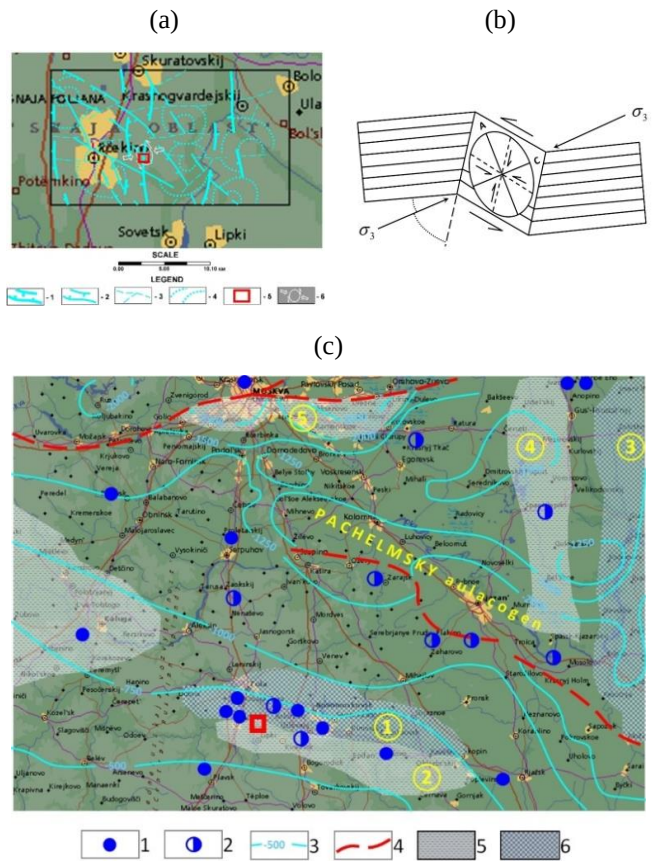

Figure 3. Elements of regional geostructural reconstruction: (a) tracing the terrestrial fractures within the central part of Tula Region (1-4 – different-ranked elements of fault tectonics with ranging corresponding to the degree of particular fracture fragmentation; 5 – arch elements organized into ring structures; 6 – position of the analyzed area; white lines indicate reconstruction of normal stresses according to the model of deformation ellipsoid in the vicinity of the area marked by blue contour); (b) a model of the deformation ellipsoid [31] where long axis of the ellipsoid is oriented along bisector of acute angle between conjugated fissures (approximately at 60^0 to each other) with shear kinematics; 3 – normal stresses; (c) fragment of tectonic map of the Russian Platform (according to K.Yu. Volkov [32]) (1 – wells opening the crystalline basement (numerator is the roof depth marker; and denominator is total drilling depth of); 2 – wells where the total drilling depth is more shallow than the depth of crystalline basement roof; 3 – isohypse of roof of crystalline basement according to combination of drilling data and seismic prospecting; 4 – the same as 3 but according to the data resulting from gravity survey; 5 – deep fault; 6 – local synforms; and 7 – local antiforms. Numbers in circles: 4 – Trufano-Paveletskaya uplift zone; 5 – Shchekino-Gorlovskaya zone of troughs; 6 – Oksko-Tsinisky swell; 7 – Vladimir-Shilovsky trough; 8 – Moscow graben)

Taking into account the fact, one can suppose northeastern strike of axis along which the normal stresses are applied to rock massif within the investigated area (Fig. 3b). Then, applying the concept of conjugate fractures and associated model of ellipsoid of deformations (Fig. 3a), the generalized field of normal and shear stresses in projection onto cartographical plane of the analyzed territory is derived.

The abovementioned gradient operators and integrating procedure have been applied for a mid-scale detailing of the geostructural image while undertaking efforts to identify the generalized contour of the stressed rock massif. As a result, the image of elliptical structure was mapped, fragmented along the set of sublatitudinal geodynamic zones, along the zones of northeastern and, to a lesser extent, north-western strike (Fig. 4a).

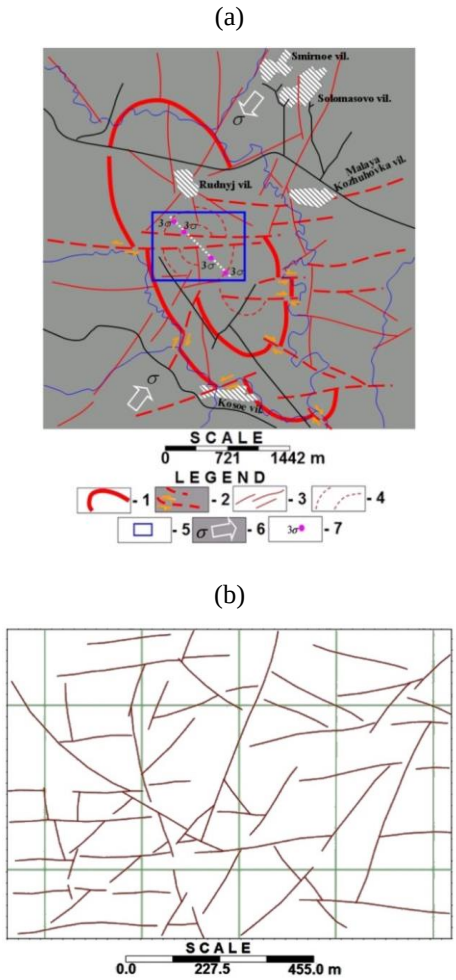

Figure 4. Mid-scale and detailed geostructural reconstructions in the vicinity of the construction area: (a) detailing the image of ellipsoid of deformations (1 – elliptical contour of the stressed rock massif; 2 – geodynamic zones with shear kinematics; 3 – elements of fracture tectonics of unknown kinematics (low-contrast); 4 – arch regional lineaments; 5 – the analyzed area contour; 6 – normal stress; 7 – generalized position of stress concentrators within the analyzed area); and (b) large-scale geodynamic zones detailing based on combined decoding of remote sensing data (IR-band) and digital elevation model

The elliptical structure contour is supposed to be the boundary of certain weakened zone [33] making it possible to apply the analogy with model of development of stress concentrators to localize areas with increased risk of the rock massif destruction. The mentioned model is related to the simplest mechanical formation, on the surface of which normal stresses σ are applied. It causes stress concentrator appearing in the bulk of formation, in small vicinity of cavity (weakened zone), and the propagation of zone of material plastic flow developing into a fissure. Figure 4b shows the large-scale data (approximately 1:14000) obtained during the final stage of geostructural estimations in a cartographic

plane. Smoothed morphology of the Earth's relief implies the use of multiseasonal remote sensing images and digital elevation model to contrast the latest vertical subsidences within the investigated area.

Schematic map of geodynamic zones in Figure 5b is generalized up to the level of lineament density map (Fig. 3c) and substantiated at the stage of morphotectonic analysis (Fig. 5a). First of all, one can see the manifestation of ring structure within the map of geoblock structuring (Fig. 5a), which substantiate the middle-scale reconstructions (Fig. 4a). The area of contact of more than two geoblocks is considered as a forecast indicator with regard to localization of areas of possible earthquake source (PES) where significant variation of entropy parameter (i.e. a parameter of spatial stationarity of the Earth's relief) takes place (Fig. 5b). Final stage of the analysis involved comparison of the ranked PES areas with the lineament density map, where the maxima identified areas of increased fragmentation of geological environment. The coincidences of PES areas of 3rd and 4th ranks with the located maxima of lineament density field were indicated by triangular markers and included in the final map of prognostic areas of seismogenic risk (Fig. 5c). It is particularly remarkable that the majority of the selected PES areas belong to previously specified subsidence zones.

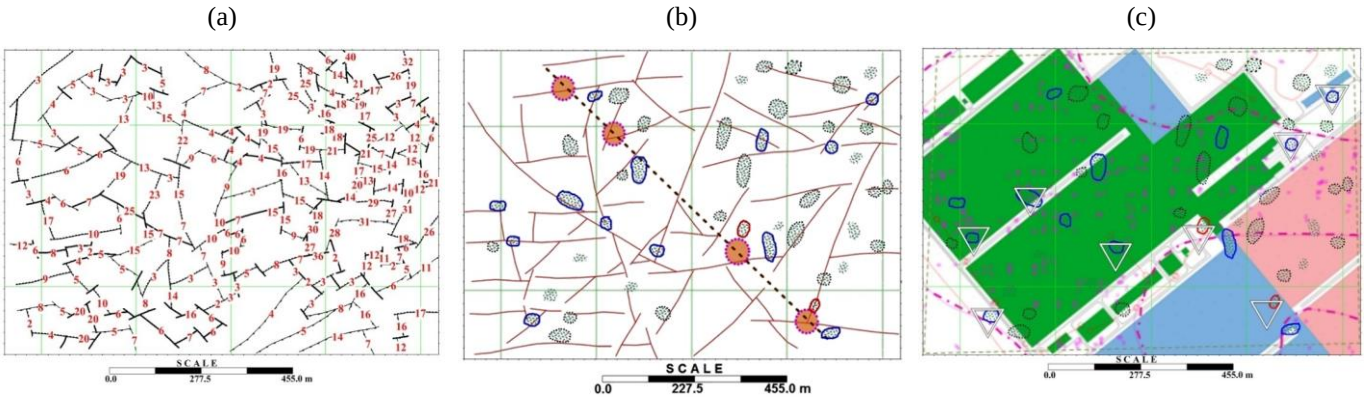

Figure 5. Detailed morphostructural forecast: (a) geoblock fragmentation of the analyzed area, simulated at a stage of morphotectonic analysis combined with ranking elements (the boundaries are marked by the value of difference of average entropy value when moving from one geoblock to another); (b) forecast of potential PES zones against the background of large-scale geostructural reconstruction (the most significant risk areas are: blue contours being 3rd rank, marking the attraction to the nodes of intersection of geodynamic zones; red contours being 4th rank of maximum significance, marking the attraction to mentioned as well as to the stress concentrators (orange circles)); (c) predictive map of PES area location. The background of map reflects the principal position of a mine working boundaries; the pink dash-dotted line marks the zone of rocks subsidence. The classification of PES areas of 3rd and 4th ranks (marked with triangles) is based on criterion of coincidence of the largest number of indicative detection

Considering the independence of decoding criteria, combination of heterogeneous data (remote sensing images and digital elevation model) at different scale levels as well as application of mutually verifying interpretation methods, the forecasting map in Figure 6c can be considered as the completed result requiring substantiation by geophysical estimations.

4. Discussion

Taking into account the last thesis about geophysical detailing, the interpretation procedure was extended by solution of inverse problem based on the recalculation of digital elevation model of the Earth's relief in the volume of geological environment. The final aim of the procedure was geostructural reconstruction in the plane of vertical cross-section (Fig. 6). The algorithm of recalculation used wave analogies was described above.

In contrast to the reconstructions, based on geophysical (i.e. seismic and electrical) data, in the context of the case, the inverse problem is solved by the less rigorous model, where h depth is computed as a relative parameter with application of empirical proportion $h = \frac{\lambda}{\sqrt{2}}$ between the linear size λ of landscape anomalies and the depth of their endogenous roots. The effect of multilevel isostatic compensation, widely known in gravity prospecting, is supposed to be the physical model: the larger the size of positive or negative form of the Earth's relief is, the deeper the form compensated hydrostatically is (see the Pratt and Airy model). The profile for deep reconstruction and, accordingly, for the selection of absolute heights of the Earth's surface relief is selected in a sublatitudinal direction, crossing central share of the analyzed area (Fig. 6a). The signal detail is the first meters, which allows speaking about the representativeness of geostructural image in small parts of the cross-section. The selected PES areas belong the zones of regional faults manifestation, to structural-constitutional complexes thinning (sharp lateral variability of their composition), and to the elements of the increased permeability zones. The deep reconstruction of cross-section in Figure 6b is considered to be independent way of presorting PES areas localized at the stage of reconstruction in cartographic plane (Fig. 5b). According to industrial experience, the approach is popular to estimate objects having neither engineering nor geophysical data due to the limited access and complicated terrain.

Upon achieving the early forecast, the authors implemented seismic measurements within the industrial order (Fig. 7), organized according to the common-depth-point (CDP) technique [34], [35]. The measurement system was central, with no offset. The spacing between geophones was equal to 2.5 m, and the step of vibropoints (VP) was equal to 5 m. 48-channel array, composed by SGD-AD ground geophones with eigen 10 Hz frequency, was used.

(a)

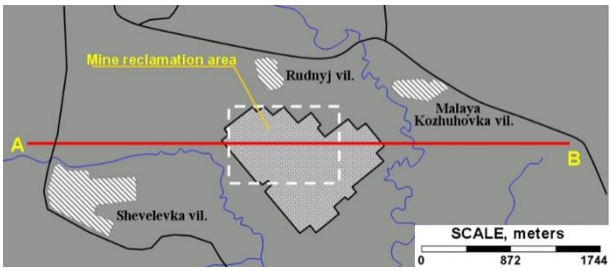

(b)

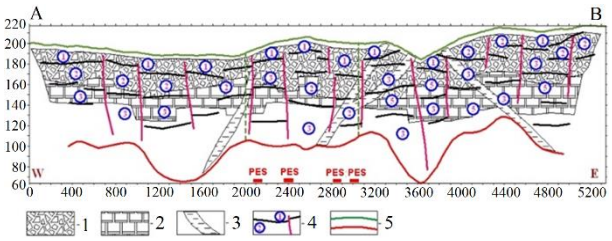

Figure 6. Example of deep geostructural reconstruction along AB profile: (a) geographical reference of AB profile with regard to the boundaries of the area of interest; (b) image of geostructural reconstruction in vertical cross-section plane; 1 and 2 – stratification elements; 3 – through zones of the increased permeability of geological environment; 4 – interfaces (black is bedding; pink is fracture) and layer numbering; 5 – roof and subface of reconstruction (green is the Earth's relief; red is deep level of hydrostatic compensation of the Earth's relief). The vertical green dotted line marks the boundaries of the area of interest. In the lower part of the section, the positions of PES zones are marked according to Figure 5c in projection on AB profile. The scale of vertical and horizontal axes is defined in meters

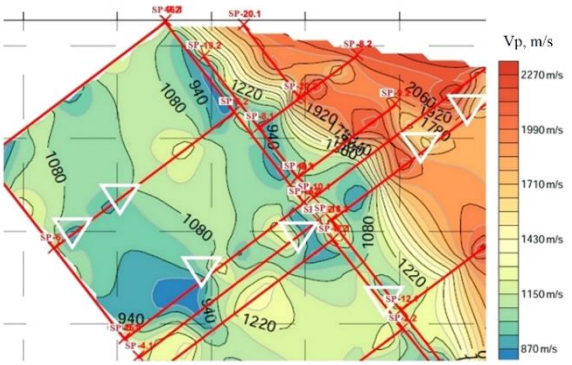

Figure 7. Fragment of the velocity model of P-wave propagation to the depth of about 20 m. Red lines mark the seismic profiles. White triangles are PES areas (according to Figure 6c). The area of scalar field of P-wave velocity coincides with the area of the early forecast in Figure 5c

The increase in CDP order at the junction of geophone arrays supposes application of additional 12 VP along the flank observation system with variable 2.5 to 57.5 m offset. Thus, CDP order changed from 12 to 24 because of low relative intensity of target wave in the fractured rocks. Office processing of field data was carried out by RadExPro software designed for integrated processing of data of surface engineering seismics as well as for quality control of field seismic data [36]. In total, during the processing, 21 sets of seismic determinations were identified fitted into three kinds of structuring of the velocity and depth propagation of wave extremum; one of them follows CDP; and two others follow refraction correlation method (RCM). Resulting from RCM interpretation, a layer which had the roof at the depth of 20 meters and increased velocity distribution within the range of 789-1317 mps was selected. The layer had wide spread occurrence within the area of interest. The comparison of location of different-ranked PES areas (Fig. 5c) and the negative anomalies of P-wave velocity (i.e. zones of increased watering and deconsolidation shown in Figure 7) demonstrates significant spatial correlation. The correlation especially concerns 3rd and 4th rank PES zones as well as the result of their presorting according to the lineament density map. Thus, objectivity of the early forecast implication concerning PES area method, based upon qualitative and quantitative analysis of remote sensing data and digital elevation model of the Earth's relief, can be noted.

5. Conclusions

The analysis has been performed based on the transition from small to large scale: from the location of polygon position at the contact of Precambrian structures up to deriving the particular identification of regional fault in the vicinity of the area of interest. Despite the seismologically stable structural-tectonic position, the area is placed in the zone of widespread limestone which causes karst development and final reduction in the stability of the upper part of geological cross-section. The karst development intensity and final high-amplitude subsidence of the Earth's surface are associated with both the activation of tectonic faults and exogenous processes. Against the background of fast treated karstogenic formations, appropriate erosion processes, and watering initiate continuous dynamics of karst. The processes reflect the importance of the morphostructural and geodynamic analysis of remote sensing data and digital elevation model of the Earth's surface, focused on mapping the inherited manifestation of elements of fracture tectonics and the geoblock structure. The analysis is especially effective under conditions of initially smoothed relief and developed sea sediments being wide spread in the area of interest. The analyzing technique includes qualitative and quantitative interpretation approaches where the first one is focused on lateral tracing of heterogeneities, whereas the second one is reduced to the deep reconstruction. In the case of quantitative interpretation, digital elevation model reflecting functional dependence between landscape and pre-Quaternary geology is considered within the concept of wave structuring of the Earth's crust.

The importance of the considered approach is explained by remote sensing data and digital elevation model related to broad access materials for any continental part of the Earth's crust. The mentioned lateral tracing is based on parametric decoding to solve the problem of tracing geodynamic zones; geoblock structure reconstructing as well as patterns in the stress field of rock massif. The positions of possible focuses of secondary earthquakes are substantiated both by decoding at different scale levels and by applying functionally independent parametric estimations. Deep reconstructions rely upon the wave model developed in publications by O.V. Petrov and I.B. Movchan [37] where the jump-like changes in standing wave lengths are associated with the law of their dispersion reflecting position of the interfaces in the

stratified geological environment. Subvertical position of the interfaces is interpreted as a response of through zones of the increased geological environment permeability. Correlation of potential sources of secondary earthquakes with the zones of the enhanced permeability helps make highly reliable prediction of areas with the increased seismological magnitude. Subsequent industrial activity by the shallow seismic technique confirms the reliability of PES areas localized at a stage of remote sensing data processing combined with the digital elevation model.

Acknowledgements

This work has been carried out without any funding from a grant or scientific project.

References

[1] Eppelbaum, L.V. (2007). Localization of ring structures in Earth's environment. *Journal of Archaeological Science of the Slovakian Academy of Sciences*, (XLI), 145-148.

[2] Koronovsky, N.V., Bryantseva, G.V., Goncharov, M.A., Naimark, A.A., & Kopaev, A.V. (2014). Lineaments, planetary jointing, and the regmatic system: Main points of the phenomena and terminology. *Geotectonics*, (48), 151-162. https://doi.org/10.1134/S0016852114020058

[3] Putikov, O.F., & Senchina, N.P. (2015). Precise solution of the system of nonlinear differential equations in partial derivatives of the theory of geoelectrochemical methods. *Doklady Earth Sciences*, *463*(1), 726-727. https://doi.org/10.1134/S1028334X15070132

[4] Ulomov, V.I., & Bogdanov, M.I. (2007). On the software and mathematical support for development of the maps of probabilistic seismic zoning according to OSR-97 technique. *Geophysical Research: Collection of Scientific Papers of the Institute of Physics of the Earth RAS*, (7), 29-52.

[5] Giardini, D., Gruenthal, G., Shedlock, K., & Zhang, P. (2003). The GSHAP global seismic hazard map. *International Journal of Geophysics*, *81*(B), 1239-1244. https://doi.org/10.1016/s0074-6142(03)80188-2

[6] Gospodarikov, A.P., & Chi, T.N. (2019). The impact of earthquakes on the tunnel from Hanoi metro system when the tunnel has a horseshoe shape cross-section. *International Journal of Civil Engineering and Technology*, *10*(02), 79-86.

[7] Kheraskova, T.N., Andreeva, N.K., Vorontsov, A.K., & Kagramanyan N.A. (2005). Evolution of Moscow sedimentary basin in early Paleozoic. *Lithology and Mineral Resources*, *40*(2), 150-166. https://doi.org/10.1007/s10987-005-0016-x

[8] Sokolov, E.M., Dmitrakov, A.V., Simakin, A.F., & Reshetov, V.V. (2000). *Geoecology of the economic complex of Tula and its region*. Tula, Russia Federation: Tula State University.

[9] Danilev, S.M., & Danileva, N.A. (2018). Characteristics electromagnetic waves of GPR data for study of hidden cavities in the engineering objects. *Proceedings of the 14th Conference and Exhibition on Engineering and Mining Geophysics 2018*, 1-4. https://doi.org/10.3997/2214-4609.201800540

[10] Danilev, S.M., & Danileva, N.A. (2019). Perspective electrical exploration the dams of gypsum accumulator in the framework for geotechnical monitoring. *Proceedings of the 15th Conference and Exhibition on Engineering and Mining Geophysics 2019*, 1-7. https://doi.org/10.3997/2214-4609.201901716

[11] Ostrovskaya, E.V. (2002). Some problems of ecology of natural waters of Novomoskovsk district of Tula region. *Journal of Mining Institute*, (152), 9-41.

[12] Clifford, F.D., & Williams, P. (2007). *Karst hydrogeology and geomorphology*. New York, United State: John Wiley. https://doi.org/10.1002/9781118684986

[13] Afanasiadi, E.I., Gryaznov, O.N., Dubeykovsky, S.G., & Neshetkin, O.B. (2003). Limestone karst of the East Ural Region. *Journal of Mining Institute*, (153), 46-50.

[14] Pashkevich, M.A., & Petrova, T.A. (2019). Development of an operational environmental monitoring system for hazardous industrial facilities of Gazprom Dobycha Urengoy. *Journal of Physics: Conference Series*, (1384), 1-7. https://doi.org/10.1088/1742-6596/1384/1/012040

[15] Egorov, A.S., Vinokurov, I.Y., Belevskaya, E.S., & Kalenich, A.P. (2016). Deep structure of the Barents-Kara region according to geophysical investigations along 1-AR and 2-AR geotravers. *Proceedings of the 7th Eage Saint Petersburg International Conference and Exhibition "Understanding the Harmony of the Earth's Resources through Integration of Geosciences"*, 728-732. https://doi.org/10.3997/2214-4609.201600173

[16] Rakhil, K.R., Kishan, D., & Sarup, J. (2015). Lineament extraction and lineament density assessment of Omkareshwar M.P., India, using GIS Techniques. *International Journal of Engineering and Management Research*, *5*(3), 717-720. https://doi.org/10.30536/j.ijreses.2016.v13.a2704

[17] Yakovleva, A.A., Movchan, I.B., Misseroni, D., Pugno, N.M., & Movchan, A.B. (2021). Multi-physics of dynamic elastic metamaterials and earthquake systems. *Frontiers in Materials*, (7), 489. https://doi.org/10.3389/fmats.2020.620701

[18] Gupta, R.P. (2003). *Remote sensing: Geology*. Berlin, Germany: Springer-Verlag. https://doi.org/10.1007/978-3-662-05283-9

[19] Nugroho, U.C., & Tjahjaningsih, A. (2016). Lineament density information extraction using DEM SRTM data to predict the mineral potential zones. *International Journal of Remote Sensing and Earth Sciences*, *13*(1), 67-74. https://doi.org/10.30536/j.ijreses.2016.v13.a2704

[20] Kennelly, P.J. (2008). Terrain maps displaying hill-shading with curvature. *Geomorphology*, *102*(3-4), 567-577. https://doi.org/10.1016/j.geomorph.2008.05.046

[21] Dahlhaus, R., Kurths, J., Maass, P., & Timmer, J. (2021). *Mathematical methods in time series analysis and digital image processing*. Berlin, Germany: Springer. https://doi.org/10.1007/978-3-540-75632-3

[22] Nunez, I., & Ferrari, J.A. (2007). Differential operator approach for Fourier image processing. *Journal of the Optical Society of America*, *24*(8), 2274-2279. https://doi.org/10.1364/JOSAA.24.002274

[23] Singhroy, V.H., & Pilkington, M. (2014). Geological mapping using Earth's magnetic field. *Encyclopedia of Remote Sensing*, 232-237. https://doi.org/10.1007/978-0-387-36699-9_38

[24] Grazzini, J., Turiel, A., & Yahia, H. (2002). Entropy estimation and multiscale processing in meteorological satellite images. *Proceedings of the 16th International Conference on Pattern Recognition*, (3). https://doi.org/10.1109/ICPR.2002.1048103

[25] Muhammad, E.M.N., Muhammad, S.S., Arif, H., Wildan, N.H., Benyamin, S., Mirzam, A., & Alfend, R. (2020). Automatic and manual fracture-lineament identification on digital surface models as methods for collecting fracture data on outcrops: case study on fractured granite outcrops, Bangka. *Journal of Frontiers in Southeast Asian Geosciences*, (17). https://doi.org/10.3389/feart.2020.560596

[26] Petrov, O.V. (2019). *The Earth's dissipative structures: Fundamental wave properties of substance*. Cham, Switzerland: Springer Geophysics. https://doi.org/10.1007/978-3-319-93614-7_6

[27] Petrov, O.V. (2021). *The Earth's free oscillations*. Springer. Berlin, Germany: Springer. https://doi.org/10.1007/978-3-030-67517-2

[28] Petrakov, D.G., Kupavykh, K., & Kupavykh, A. (2020). The effect of fluid saturation on the elastic-plastic properties of oil reservoir rocks. *Curved and Layered Structures*, (7), 29-34. https://doi.org/10.1515/cls-2020-0003

[29] Ribe, N.M. (2001). Bending and stretching of thin viscous sheets. *Journal of Fluid Mechanics*, (433), 135-160. https://doi.org/10.1017/S0022112000003360

[30] Aleksanova, E., Varentsov, I.M., Vereshchagina, M., & Kulikov, V.A. (2010). Electormagnetic sounding of the sedimentary cover and consolidated crust in the transition zone from the Moscow Syneclise to the Voronezh Anteclise: Problems and prospects. *Izvestiya, Physics of the Solid Earth*, *46*(8), 707-716. https://doi.org/10.1134/S1069351310080070

[31] Mulchrone, K.F., & Talbot, Ch.J. (2014). Constraining the strain ellipsoid and deformation parameters using deformed single layers: A computational approach assuming pure shear and isotropic volume change. *Journal of Structural Geology*, (52), 194-206. https://doi.org/10.1016/j.jsg.2014.02.002

[32] Volkov, K.Yu. (1965). *Schematic map of roof relief of crystalline basement of Moscow syneclise and Ryazan-Saratov trough*. Moscow, Russian Federation: GURTs.

[33] Mazurov, B.T., Mustafin, M.G., & Panzhin, A.A. (2019). Estimation method for vector field divergence of Earth crust deformations in the process of mineral deposits development. *Journal of Mining Institute*, *238*(4), 376-383. https://doi.org/10.31897/pmi.2019.4.376

[34] Gorelik, G.D., Budanov, L.M., Ryabchuk, D., Zhamoida, V., & Neevin, I. (2019). Application of CDP seismic reflection method in buried paleo-valley study. *Proceedings of the 15th Conference and Exhibition on Engineering and Mining Geophysics 2019*, 1-7. https://doi.org/10.3997/2214-4609.201901777

[35] Sloan, S.D., Tsoflias, G.P., & Steeples, D.W. (2010). Ultra-shallow seismic imaging of the top of the saturated zone. *Geophysical Research Letters*, *37*(7), L07405. https://doi.org/10.1029/2010GL043034

[36] Lalomov, D., Glazunov, V., Tatarskiy, A., Burlutsky, S., & Efimova, N. (2019). Methodical features of studying the geological structure of the coastal part of the sea of Okhotsk based on the integration of continu-

ous aquatic electrical sounding and seismoacoustics data. *Proceedings of the 25th European Meeting of Environmental and Engineering Geophysics, Held at Near Surface Geoscience Conference and Exhibition 2019*, 1-5. https://doi.org/10.3997/2214-4609.201903466

[37] Movchan, I.B., & Yakovleva, A.A. (2020). Wave analogies in the quantitative interpretation of potential fields. *International Journal of Advanced Trends in Computer Science and Engineering*, *9*(2), 1793-1799. https://doi.org/10.30534/ijatcse/2020/136922020

Випереджувальна оцінка сейсмічної небезпеки на прикладі стику Воронезького масиву та Московської западини

І. Мовчан, О. Яковлєва, О. Мовчан, З. Шайгаллямова

Мета. Розробка системного підходу для випереджаючого прогнозу ділянок підвищеної сейсмічної небезпеки, що характеризуються малою стійкістю гірського масиву по відношенню до зовнішніх навантажень.

Методика. Проведено оцінку керна свердловин до глибини 30 м, а також накопичення сейсмологічних спостережень. Для досліджень застосовані комплекси методів польової геофізики, матеріали дистанційного зондування і цифрова модель рельєфу земної поверхні, прийоми якісної та кількісної інтерпретації.

Результати. Сформована карта сейсмічної небезпеки в термінах прирощення сейсмічної інтенсивності та в одиницях зміщення ґрунту, що є надійним, але дорогим результатом, що вимагає випереджальних оцінок позиції ділянок підвищеної сейсмічної небезпеки для згущення мережі геофізичних вимірювань в околиці цих ділянок для їх подальшої кількісної характеристики. Визначено, що рідка мережа свердловин і окремі геофізичні профілі, які прокладаються в умовах складного ландшафту, не здатні локалізувати ділянки високої сейсмічної небезпеки, щоб сфокусувати увагу будівельників на посиленні конкретних елементів конструкцій, що зводяться. Встановлено, що кінцевий результат прогнозних побудов має форму схеми розподілу локальних ділянок зниженої стійкості верхньої частини геологічного розрізу, які підтверджуються наступними вимірами методом малоглибинної сейсміки (ЗГТ). Зіставлення можливих вогнищ вторинних землетрусів із зонами підвищеної проникності дозволяє з високою надійністю прогнозувати області підвищеної сейсмологічної магнітуди.

Наукова новизна. Вперше адаптовані способи інтерпретації для параметричного опису непотенційних геополів (оптичної щільності дистанційної основи, відносних перевищень земного рельєфу), прийнятих в обробці потенційних полів, із застосуванням хвильових аналогій.

Практична значимість. Розроблено методику, що дозволяє оптимізувати польові геолого-геофізичні роботи за площею та кількістю свердловин і вимірювальних пікетів в умовах обмеженості обсягу апріорних даних.

Ключові слова: *тріщинуватість, сейсмічне районування, ландшафт, карст, цифрова модель дешифрування*

Опережающая оценка сейсмической опасности на примере стыка Воронежского массива и Московской впадины

И. Мовчан, А. Яковлева, А. Мовчан, З. Шайгаллямова

Цель. Разработка системного подхода для опережающего прогноза участков повышенной сейсмической опасности, характеризуемых малой устойчивостью горного массива по отношению к внешним нагрузкам.

Методика. Проведена оценка керна скважин до глубины 30 м, а также накопление сейсмологических наблюдений. Для исследований применены комплексы методов полевой геофизики, материалы дистанционного зондирования и цифровая модель рельефа земной поверхности, приемы качественной и количественной интерпретации.

Результаты. Сформирована карта сейсмической опасности в терминах приращения сейсмической интенсивности и в единицах смещения грунта, что является надежным, но дорогим результатом, требующим опережающих оценок позиции участков повышенной сейсмической опасности для сгущения сети геофизических измерений в окрестности этих участков для их последующей количественной характеристики. Определено, что редкая сеть скважин и отдельные геофизические профили, прокладываемые в условиях сложного ландшафта, не способны локализовать участки высокой сейсмической опасности, чтобы сфокусировать внимание строителей на усилении конкретных элементов возводимых конструкций. Установлено, что конечный результат прогнозных построений имеет форму схемы распределения локальных участков пониженной устойчивости верхней части геологического разреза, которые подтверждаются последующими измерениями методом малоглубинной сейсмики (ОГТ). Сопоставление возможных очагов вторичных землетрясений с зонами повышенной проницаемости позволяет с высокой надежностью прогнозировать области повышенной сейсмологической магнитуды

Научная новизна. Впервые адаптированы способы интерпретации для параметрического описания непотенциальных геополей (оптической плотности дистанционной основы, относительных превышений земного рельефа), принятых в обработке потенциальных полей, с применением волновых аналогий.

Практическая значимость. Разработана методика, позволяющая оптимизировать полевые геолого-геофизические работы по площади и по количеству скважин и измерительных пикетов в условиях ограниченности объема априорных данных.

Ключевые слова: *трещиноватость, сейсмическое районирование, ландшафт, карст, цифровая модель дешифрирование*